

Passivity-based Sliding-mode Control Design for Optimal Power Extraction of a PMSG based Variable Speed Wind Turbine

Bo Yang*, Tao Yu†, Hongchun Shu*, Yuming Zhang*, Jian Chen‡, Yiyan Sang§, Lin Jiang§

Abstract

This paper proposes a novel passivity-based sliding-mode control (PB-SMC) scheme of permanent magnetic synchronous generator (PMSG) for maximum power point tracking (MPPT). A storage function is constructed based on the passivity theory at first, in which the beneficial system nonlinearities, e.g., which can make the derivative of storage function to be more negative, are carefully remained so as to improve the system damping while all the other system nonlinearities are fully removed. Then, an additional input is used to lead the closed-loop system to be output strictly passive via energy reshaping, meanwhile a sliding-mode control (SMC) is incorporated to greatly enhance the system robustness against various uncertainties of PMSG. Hence, PB-SMC can simultaneously own the promising merits of improved system damping and significant robustness, together with a globally consistent control performance under various operation conditions. Case studies including step change of wind speed, stochastic wind speed variation, pitch angle variation, and generator parameter uncertainties, are undertaken which verify the effectiveness and superiority of PB-SMC compared to that of other typical controllers. Lastly, a dSpace based hardware-in-loop (HIL) test is carried out to validate the implementation feasibility of PB-SMC.

Keyword PMSG, MPPT, passivity-based sliding-mode control, energy reshaping, storage function

*Bo Yang, Hongchun Shu, and Yuming Zhang are with the Faculty of Electric Power Engineering, Kunming University of Science and Technology, 650500, Kunming, China.

†Tao Yu is with the School of Electric Power Engineering, South China University of Technology, Guangzhou, China. (corresponding author, Tao Yu, Email: taoyu1@scut.edu.cn)

‡Jian Chen is with the School of Electrical Engineering, Yancheng Institute of Technology, Yancheng, 224051, China

§Yiyan Sang and Lin Jiang are with the Department of Electrical Engineering & Electronics, University of Liverpool, Liverpool, L69 3GJ, United Kingdom.

1 Introduction

Sustainable energy has been undoubtedly regarded as a promising alternative energy source as conventional fossil fuels are limited and continuously cause ever-growing pollution issues. Currently, one of the most favorable sources of sustainable energy is wind energy which has the merits of abundance, cleanness, and wide distribution [1–5]. The variable speed wind turbine systems are usually based on doubly-fed induction generator (DFIG) [6] or permanent magnet synchronous generator (PMSG) [7]. Recently, the application of PMSG has been considerably increased thanks to its elegant features of simple structure, efficient energy production, gearless construction, self-excitation, and low noise [8]. Therefore, it is expected that a growing number of PMSG will be employed in wind energy conversion systems (WECS) around the globe.

In WECS, an effective optimal power extraction with low implementation costs, also known as maximum power point tracking (MPPT) [9,10] control strategy, is essential to improve the operation efficiency. Conventional vector control (VC) associated with proportional-integral (PI) control loops are popularly adopted and widely implemented in practice due to its elegant advantages of simple structure [11]. However, its control design is mainly based on a linearized model at a specific operation point, while its control performance might be significantly degraded or even lead to a system instability as the operation condition of PMSG often varies. In order to remedy this inherent flaw of PI control, a virtually adaptive PI controller was proposed with a wavelet neural network (WNN) to dynamically adjust the PI gains through online training [12]. Moreover, reference [13] developed a back-propagation learning algorithm with modified particle swarm optimization (MPSO) to tune the PI parameters of PMSG, such that a loss-minimization control of MPPT can be realized. In addition, a fuzzy fractional order PI+I controller was designed with a particle swarm optimization (PSO) to realize MPPT of PMSG [14]. Besides, an improved bacterial foraging optimization (BFO) technique was employed to optimize PI parameters which aims to extract the maximum power from the wind [15].

On the other hand, nonlinear control has been largely investigated to handle the above thorny problems resulted from one-point linearization. Reference [16] reported a feedback linearization control (FLC) which globally removes all the nonlinearities to achieve MPPT while PSO is used to optimize the control gains of FLC [17], such that a consistent control performance under various operation conditions can be realized. In work [18], a model predictive control (MPC) and dead-beat predictive control strategies were developed to forecast the possible future behaviour of the control variables of PMSG. Additionally, a fuzzy integral sliding-mode current controller was proposed to extract the optimal wind power and eliminate the high-order voltage harmonics of PMSG [19]. Further, literature [20] presented a multiple-input-

multiple-output high-order sliding-mode control (SMC) scheme so as to regulate the active and reactive power delivered to the power grid, minimize the resistive losses of the generator and maintain important internal variables into the desired range. Meanwhile, an enhanced exponential reaching law based SMC was devised for PMSG to reduce the malignant chattering issues and to improve total harmonic distortion property [21]. Meanwhile, literature [22] presented a robust nonlinear predictive control (RNPC) to adjust the rectifier voltage amplitude and stator current in the face of external disturbances, which implementation feasibility was validated by dSPACE hardware. Besides, a nonlinear Luenberger-like observer was designed to estimate the mechanical variables by only the measurement of electrical variables of PMSG to achieve MPPT [23]. Moreover, an artificial neural network (ANN)-based reinforcement learning (RL) was employed for PMSG to achieve MPPT, which enables the WECS to behave like an intelligent agent with memory to learn from its own experience, thus improving the learning efficiency [24].

However, the aforementioned approaches usually ignore the physical property of PMSG during the control design. Inspiringly, passive control (PC) provides an invaluable insight of physical features of a given engineering problem so as to achieve an optimal control. It actually views a dynamical system as an virtual energy-transformation device, which can decompose a complex nonlinear system into several simpler subsystems that, upon careful interconnection, and adds up their local/distributed energies to determine the overall system's behaviour [25]. PC was adopted to synthesize a controller for the active power of DFIG via energy reshaping in the context of extreme operating conditions [26]. Based on interconnection and damping assignment, PC was employed to achieve MPPT of PMSG [27]. Other engineering applications of PC can be referred to voltage source converter based high-voltage direct-current (VSC-HVDC) systems [28], synchronous generator [29], marine vehicle [30], photovoltaic/battery hybrid power source [31], fuel cell and supercapacitors [32], etc.

One obvious drawback of PC is the fact that it usually requires an accurate system model in order to analyze the physical property and roles of each terms of a dynamical system, thus its practical application is somehow limited resulted from the lack of robustness, particularly for PMSG in which the wind speed is highly stochastic and accurate generator parameters are generally unavailable. Such challenging obstacle motivates this paper to develop a robust PC scheme to enhance the robustness in the context of wind speed randomness and generator parameter uncertainties. The novelty and contribution of this paper can be summarized as the following three aspects:

- Based on passivity theory, a storage function is constructed for PMSG to achieve MPPT, which is in the form of the sum of the resistor heat produced by d-axis current flowing through a virtual unit resistance, kinetic energy of the shaft system, and the accelerating torque energy. Hence, the physical

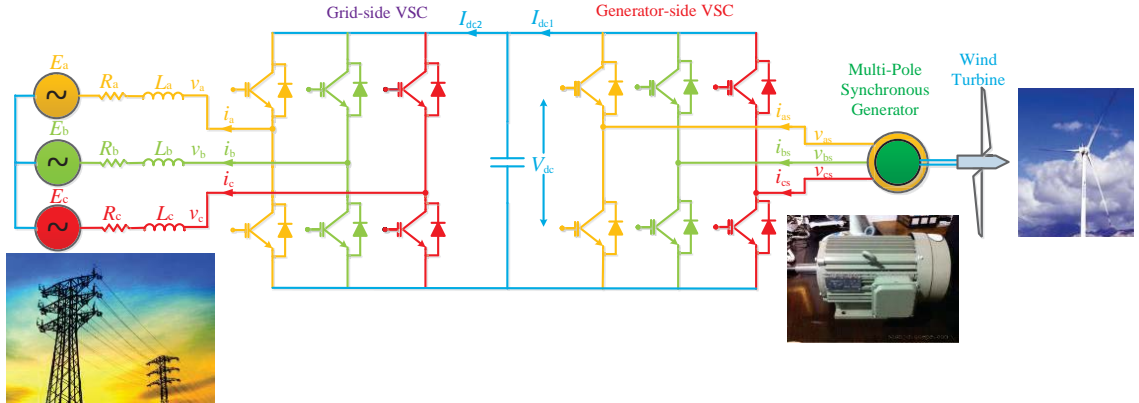


Figure 1: The configuration of a PMSG directly connected to a power grid.

property of PMSG is thoroughly analyzed;

- The beneficial terms are wisely exploited to improve the system damping while an addition input is introduced to lead the closed-loop system to be output strictly passive via energy reshaping, which guarantee a rapid error tracking convergence of mechanical rotation speed and reactive power;
- An SMC is incorporated into original PC which attempts to considerably enhance the robustness of the proposed approach in the presence of stochastic wind speed and generator parameter uncertainties.

The remaining of this paper is organized as follows: Section II develops the PMSG model and Section III provides the design procedure of PB-SMC for MPPT of PMSG. Then, case studies are undertaken in Section IV while hardware-in-loop (HIL) test is carried out in Section V. At last, some concluding remarks and future studies are summarized in Section VI.

2 Modelling of PMSG based Various Speed Wind Turbine

The configuration of a PMSG directly connected to an infinite power grid bus through back-to-back voltage source converter (VSC) is demonstrated by Fig. 1, in which the wind energy captured by a variable speed wind turbine is transmitted to a gearless PMSG. Here, The produced power of the generator is controlled by the generator-side VSC, while the grid-side VSC is responsible for delivering active power to the grid via the DC-link and maintaining the DC-link voltage. Two VSCs are controlled separately and the dynamics of the PMSG and the power grid is decoupled via the DC-link. As the MPPT of PMSG mainly relies on the control of the generator-side VSC, the dynamics of grid-side VSC is ignored in this paper.

2.1 Wind turbine model

In general, the aerodynamics of wind turbine is normally described by a power coefficient $C_p(\lambda, \beta)$, which is usually an algebraic function of both blade pitch angle β and tip-speed-ratio λ , with λ being defined as follows

$$\lambda = \frac{\omega_m R}{v_{\text{wind}}} \quad (1)$$

where ω_m denotes the mechanical rotation speed of wind turbine and v_{wind} represents the wind speed; R is the blade radius of wind turbine. According to the wind turbine dynamics, a generic equation employed to describe the power coefficient $C_p(\lambda, \beta)$ can be written as

$$C_p(\lambda, \beta) = c_1 \left(\frac{c_2}{\lambda_i} - c_3\beta - c_4 \right) e^{-\frac{c_5}{\lambda_i}} \quad (2)$$

with

$$\frac{1}{\lambda_i} = \frac{1}{\lambda + 0.08\beta} - \frac{0.035}{\beta^3 + 1} \quad (3)$$

The coefficients c_1 to c_5 are selected as $c_1=0.22$, $c_2=116$, $c_3=0.4$, $c_4=5$, and $c_5=12.5$, respectively [16,33].

Besides, the mechanical power extracted by the wind turbine from the wind energy can be calculated by

$$P_m = \frac{1}{2} \rho \pi R^2 C_p(\lambda, \beta) v_{\text{wind}}^3 \quad (4)$$

where ρ is the air density. It is worth noting that this paper focuses on the MPPT of PMSG, thus the wind turbine merely operates in the sub-rated speed range while its pitch control is deactivated for the whole operation of PMSG.

2.2 Permanent magnetic synchronous generator model

The PMSG model is modeled as the same as that of permanent magnetic synchronous machine (PMSM).

The voltage and torque equations of the PMSM in the d-q reference frames are expressed as [16,33]

$$V_d = i_d R_s + L_d \frac{di_d}{dt} - \omega_e L_q i_q \quad (5)$$

$$V_q = i_q R_s + L_q \frac{di_q}{dt} + \omega_e (L_d i_d + K_e) \quad (6)$$

$$T_e = p[(L_d - L_q)i_d i_q + i_q K_e] \quad (7)$$

where V_d and V_q are the stator voltages in the d-q axis; i_d and i_q are the currents in the d-q axis; R_s is the stator resistance; L_d and L_q are d-q axis inductances; $\omega_e = p\omega_m$ is the electrical rotation speed; K_e is the permanent magnetic flux given by the magnets; and p is the number of pole pairs.

2.3 Shaft system model

The dynamics of shaft system and mechanical torque of PMSG are given as follows [16,33]

$$J_{\text{tot}} \frac{d\omega_m}{dt} = T_m - T_e - D\omega_m \quad (8)$$

$$T_m = \frac{1}{2} \rho \pi R^5 \frac{C_p(\lambda, \beta)}{\lambda^3} \omega_m^2 \quad (9)$$

where J_{tot} is the total inertia of the drive train which equals to the summation of wind turbine inertia constant and generator inertia constant; D is the viscous damping coefficient which is taken to be 0 in this paper; T_m and T_e are the mechanical torque and electromagnetic torque of wind turbine, respectively. Moreover, electrical power $P_e = T_e \omega_e$.

In order to capture the maximum wind power, the power coefficient $C_p(\lambda, \beta)$ should be maintained at its maximum point C_p^* at various wind speed within the operation range. Particularly, maximum power coefficient C_p^* is achieved by maintaining the tip-speed-ratio λ to be equal to its optimal value λ^* and the pitch angle β at a fixed value, yields

$$C_p^* = C_p(\lambda^*) \quad (10)$$

which in turn requires the mechanical rotation speed ω_m to track its optimal reference ω_m^* as follows

$$\omega_m^* = \frac{v_{\text{wind}}}{R} \lambda^* \quad (11)$$

Here, the pitch angle is taken as $\beta = 2^\circ$, the optimal tip-speed-ratio $\lambda^* = 7.4$ while maximum power coefficient $C_p^* = 0.4019$ [16,33]. Moreover, x^* denotes the reference of variable x throughout the whole paper.

Lastly, the aim of MPPT is to track the optimal active power curve which is obtained by connecting each maximum power point (MPP) at various wind speed, as illustrated by Fig. 2. Here, the optimal

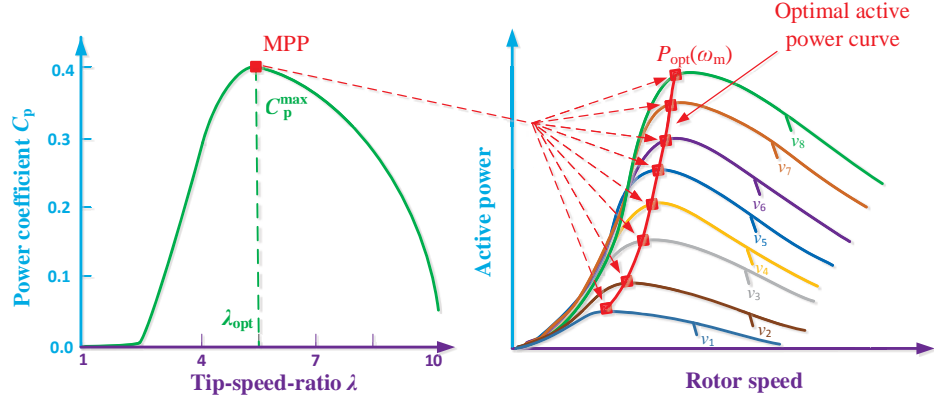


Figure 2: The optimal active power curve obtained under various wind speed.

active power curve is determined as

$$P_{\text{opt}}(\omega_m) = K^* \omega_m^3 \quad (12)$$

where $K^* = 0.5\rho\pi R^5 C_p^*/(\lambda^*)^3$ denotes the shape coefficient of optimal active power, which shows that the optimal power is proportional to the cube of mechanical rotation speed and can be interpreted as the mechanical power produced on the wind turbine in terms of mechanical rotation speed.

3 Passivity-based Sliding-mode Control of PMSG

3.1 Preliminary

Consider a dynamical nonlinear system represented with the general model

$$\begin{cases} \dot{x} = f(x, u) \\ y = h(x, u) \end{cases} \quad (13)$$

where $x \in R^n$ is the system state vector. $u \in R^m$ and $y \in R^m$ represent the input and output, respectively.

The energy balancing equation can be written as follows:

$$\underbrace{H[x(t)] - H[x(0)]}_{\text{stored}} = \underbrace{\int_0^t u^T(s)y(s)ds}_{\text{supplied}} - \underbrace{d(t)}_{\text{dissipated}} \quad (14)$$

where $H(x)$ is the stored energy function, and $d(t)$ is a nonnegative function that captures the dissipation effects, e.g., due to resistances or frictions, etc.

System (13) is defined to be output strictly passive if there exists a continuously differentiable positive semi-definite function $H(x)$ (called the storage function) such that

$$u^T y \geq \frac{\partial H}{\partial x} f(x, u) + \zeta y^T y, \quad \forall (x, u) \in R^n \times R^m \quad (15)$$

where $\zeta > 0$. In order to obtain the asymptotic stability the following lemma is needed.

Lemma 1. *Consider the system described in (13), The origin of the uncontrolled system $\dot{x} = f(x, 0)$ is asymptotically stable if the system is output strictly passive and zero-state detectable with a positive definite storage function $H(x)$. Moreover, if the storage function $H(x)$ is radially unbounded then the origin is globally asymptotic stable [25].*

If system (13) is not passive, but there exists a positive definite storage function $H(x)$ and a feedback control law $u = \beta(x) + \kappa v$ such that $\dot{H} \leq v y$, then the feedback system is passive. As a result, the feedback passivation can be used as a preliminary step in a stabilization design because of the additional output feedback

$$v = -\phi(y) \quad (16)$$

where $\phi(y)$ is a sector-nonlinearity satisfying $y\phi(y) > 0$ for $y \neq 0$ and $\phi(0) = 0$, can achieve $\dot{H} \leq -y\phi(y) \leq 0$.

3.2 PB-SMC design

The objective of PB-SMC is to carefully passivize a dynamical system with a storage function which has a minimum at the desired equilibrium point, therefore it reshapes the original system energy and assigns a closed-loop energy function equals to the difference between the energy of the system and the energy supplied by the controller, such that a significant system damping can be injected. Furthermore, a great robustness can be provided thanks to the SMC mechanism employed by the PB-SMC.

Define state variable $x = [i_d, i_q, \omega_m]^T$ and output $y = [y_1, y_2]^T = [i_d, \omega_m]^T$, the state space equation of PMSG can be calculated from (5-9), as follows

$$\dot{x} = f(x) + g_1(x)u_1 + g_2(x)u_2 \quad (17)$$

where

$$f(x) = \begin{bmatrix} -\frac{R_s}{L_d}i_d + \frac{\omega_e L_q}{L_d}i_q \\ -\frac{R_s}{L_q}i_q - \frac{\omega_e}{L_q}(L_d i_d + K_e) \\ \frac{1}{J_{\text{tot}}}(T_m - T_e) \end{bmatrix}, \quad g_1(x) = \begin{bmatrix} \frac{1}{L_d} \\ 0 \\ 0 \end{bmatrix}, \quad g_2(x) = \begin{bmatrix} 0 \\ \frac{1}{L_q} \\ 0 \end{bmatrix} \quad (18)$$

Differentiate output y until control input $u = [u_1, u_2]^T = [V_d, V_q]^T$ appears explicitly, it obtains

$$\begin{cases} \dot{y}_1 = \frac{1}{L_d}u_1 - \frac{R_s}{L_d}i_d + \frac{\omega_e L_q}{L_d}i_q \\ \ddot{y}_2 = -\frac{p i_q}{J_{\text{tot}} L_d}(L_d - L_q)u_1 + \frac{\dot{T}_m}{J_{\text{tot}}} - \frac{p}{J_{\text{tot}} L_q}[K_e + (L_d - L_q)i_d]u_2 - \frac{p i_q}{J_{\text{tot}} L_q}(L_d - L_q)(-R_s i_d + L_q \omega_e i_q) \\ \quad + \frac{p}{J_{\text{tot}} L_q}[K_e + (L_d - L_q)i_d](L_d \omega_e i_d + R_s i_q + \omega_e K_e) \end{cases} \quad (19)$$

System (19) can be then rewritten into the following matrix form

$$\begin{bmatrix} \dot{y}_1 \\ \ddot{y}_2 \end{bmatrix} = \begin{bmatrix} h_1(x) \\ h_2(x) \end{bmatrix} + B(x) \begin{bmatrix} u_1 \\ u_2 \end{bmatrix} \quad (20)$$

where

$$h_1(x) = -\frac{R_s}{L_d}i_d + \frac{\omega_e L_q}{L_d}i_q \quad (21)$$

$$h_2(x) = \frac{\dot{T}_m}{J_{\text{tot}}} - \frac{p i_q}{J_{\text{tot}} L_q}(L_d - L_q)(-R_s i_d + L_q \omega_e i_q) + \frac{p}{J_{\text{tot}} L_q}[K_e + (L_d - L_q)i_d](L_d \omega_e i_d + R_s i_q + \omega_e K_e) \quad (22)$$

and

$$B(x) = \begin{bmatrix} \frac{1}{L_d} & 0 \\ -\frac{p i_q}{J_{\text{tot}} L_d}(L_d - L_q) & -\frac{p}{J_{\text{tot}} L_q}[K_e + (L_d - L_q)i_d] \end{bmatrix} \quad (23)$$

The inverse of control gain matrix $B(x)$ can be calculated as follows

$$B^{-1}(x) = \begin{bmatrix} L_d & 0 \\ -\frac{i_q L_q (L_d - L_q)}{K_e + (L_d - L_q)i_d} & -\frac{J_{\text{tot}} L_q}{p[K_e + (L_d - L_q)i_d]} \end{bmatrix} \quad (24)$$

In order to ensure the above input-output linearization to be valid, it requires control gain matrix $B(x)$

must be nonsingular among the whole operation range, it requires

$$\det[B(x)] = -\frac{p[K_e + (L_d - L_q)i_d]}{J_{\text{tot}}L_dL_q} \neq 0 \quad (25)$$

which can be always satisfied when $K_e \neq -(L_d - L_q)i_d$.

For system (19), construct a storage function as follows:

$$H(i_d, \omega_m, T_e, T_m) = \underbrace{\frac{1}{2}(i_d - i_d^*)^2}_{\text{resistor heat}} + \underbrace{\frac{1}{2}(\omega_m - \omega_m^*)^2}_{\text{kinetic energy}} + \underbrace{\frac{1}{2}\left(\frac{T_m - T_e}{J_{\text{tot}}} - \dot{\omega}_m^*\right)^2}_{\text{accelerating torque energy}} \quad (26)$$

where i_d^* , ω_m^* , and $\dot{\omega}_m^*$ are the reference of d-axis current, mechanical rotation speed, and the derivative of mechanical rotation speed, respectively. Here, $H(i_d, \omega_m, T_e, T_m)$ is constructed in the form of the sum of the resistor heat produced by d-axis current flowing through a virtual unit resistance $r = 1 \Omega$, kinetic energy of the shaft system, and the accelerating torque energy, respectively.

Differentiate storage function $H(i_d, \omega_m, T_e, T_m)$ (26) with respect to the time, yields

$$\begin{aligned} \dot{H}(i_d, \omega_m, T_e, T_m) = & \\ & (i_d - i_d^*) \left(\frac{1}{L_d} u_1 - \frac{R_s}{L_d} i_d + \frac{\omega_e L_q}{L_d} i_q - \dot{i}_d^* \right) + \left(\frac{T_m - T_e}{J_{\text{tot}}} - \dot{\omega}_m^* \right) \left\{ -\ddot{\omega}_m^* - \frac{p i_q}{J_{\text{tot}} L_d} (L_d - L_q) u_1 + \frac{\dot{T}_m}{J_{\text{tot}}} \right. \\ & - \frac{p}{J_{\text{tot}} L_q} [K_e + (L_d - L_q) i_d] u_2 - \frac{p i_q}{J_{\text{tot}} L_q} (L_d - L_q) (-R_s i_d + L_q \omega_e i_q) + \omega_m - \omega_m^* \\ & \left. + \frac{p}{J_{\text{tot}} L_q} [K_e + (L_d - L_q) i_d] (L_d \omega_e i_d + R_s i_q + \omega_e K_e) \right\} \quad (27) \end{aligned}$$

Design PB-SMC for system (20) as follows:

$$\left\{ \begin{array}{l} u_1 = -\omega_e L_q i_q + R_s i_d^* + L_d \dot{i}_d^* + \nu_1 \\ u_2 = -\frac{L_q i_q (L_d - L_q)}{K_e + (L_d - L_q) i_d} u_1 + \frac{J_{\text{tot}} L_q}{p [K_e + (L_d - L_q) i_d]} \left\{ \ddot{\omega}_m^* - \omega_m + \omega_m^* - \frac{\dot{T}_m}{J_{\text{tot}}} + \frac{p i_q}{J_{\text{tot}} L_q} (L_d - L_q) (-R_s i_d + L_q \omega_e i_q) \right. \\ \left. - \frac{p}{J_{\text{tot}} L_q} [K_e + (L_d - L_q) i_d] (L_d \omega_e i_d + \omega_e K_e) - \frac{R_s}{J_{\text{tot}} L_q} T_m + \frac{R_s}{L_q} \dot{\omega}_m^* + \nu_2 \right\} \end{array} \right. \quad (28)$$

where ν_1 and ν_2 are additional inputs which will be designed later.

Substitute PB-SMC (28) into the derivative of storage function (27), together with electromechanical relationship (8), it gives

$$\dot{H}(i_d, \omega_m, T_e, T_m) = \underbrace{-\frac{R_s}{L_d} (i_d - i_d^*)^2 - \frac{R_s}{L_q} (\dot{\omega}_m - \dot{\omega}_m^*)^2}_{\text{beneficial terms}} + \underbrace{\frac{i_d - i_d^*}{L_d} \nu_1 + (\dot{\omega}_m - \dot{\omega}_m^*) \nu_2}_{\text{additional inputs}} \quad (29)$$

Remark 1. The first two terms of system (29) are carefully remained as they are beneficial terms which can accelerate the error tracking rate of d-axis current i_d and mechanical rotation speed ω_m . In particular, their physical property can be interpreted as the sum of the heat produced by the d-axis current i_d on the stator resistance R_s associated with d-axis inductance L_d and the accelerating torque energy associated with the stator resistance R_s and q-axis inductance L_q , such energy will be dissipated to result in a faster decrease of storage function, that is, a larger system damping. Consequently, PB-SMC can improve the transient responses of PMSG compared to that of FLC [16, 17] which fully removes the nonlinearities without any consideration or analysis of the actual role of each term existed in PMSG.

There are two objectives to design additional inputs ν_1 and ν_2 , e.g., lead the system to be output strictly passive through energy reshaping to ensure the stability of the closed-loop system and enhance system robustness by using sliding-mode mechanism. As a consequence, two sliding surfaces need to be chosen as

$$S_1 = i_d - i_d^* \quad (30)$$

$$S_2 = \rho_1(\omega_m - \omega_m^*) + \rho_2(\dot{\omega}_m - \dot{\omega}_m^*) \quad (31)$$

where ρ_1 and ρ_2 are the positive sliding surface gains. The attractiveness of the sliding surfaces (30) and (31) ensures d-axis current i_d and mechanical rotation speed ω_m can eventually track to their reference.

Consider the structure of system (29), the additional inputs can be then designed as follows:

$$\nu_1 = \underbrace{-\alpha_1(i_d - i_d^*)}_{\text{energy reshaping}} \underbrace{-\zeta_1 S_1 - \varphi_1 \text{sat}(S_1, \varepsilon_1)}_{\text{sliding-mode}} \quad (32)$$

$$\nu_2 = \underbrace{-\alpha_2(\dot{\omega}_m - \dot{\omega}_m^*)}_{\text{energy reshaping}} \underbrace{-\zeta_2 S_2 - \varphi_2 \text{sat}(S_2, \varepsilon_2)}_{\text{sliding-mode}} \quad (33)$$

where positive control gains ζ_1 , ζ_2 , φ_1 , and φ_2 are chosen to guarantee the attractiveness of sliding surfaces (30) and (31); while positive passivation gains α_1 and α_2 reshape the system into output strictly passive, such that the closed-loop system is stable; Moreover, function $\text{sat}(S_i, \varepsilon_i)$, with $i = 1, 2$, is employed to replace conventional $\text{sgn}(S_i)$ function, such that the malignant effect of chattering existed in SMC resulted from discontinuity can be reduced, which is defined as $\text{sat}(S_i, \varepsilon_i) = S_i/|S_i|$ when $|S_i| > \varepsilon_i$ and $\text{sat}(S_i, \varepsilon_i) = S_i/\varepsilon_i$ when $|S_i| \leq \varepsilon_i$; and ε_i denotes the thickness layer boundary of PB-SMC.

To this end, the overall PB-SMC structure of PMSG for MPPT is demonstrated by Fig. 3, in which mechanical rotation speed is fully decoupled from d-axis current. Lastly, the obtained control inputs (28)

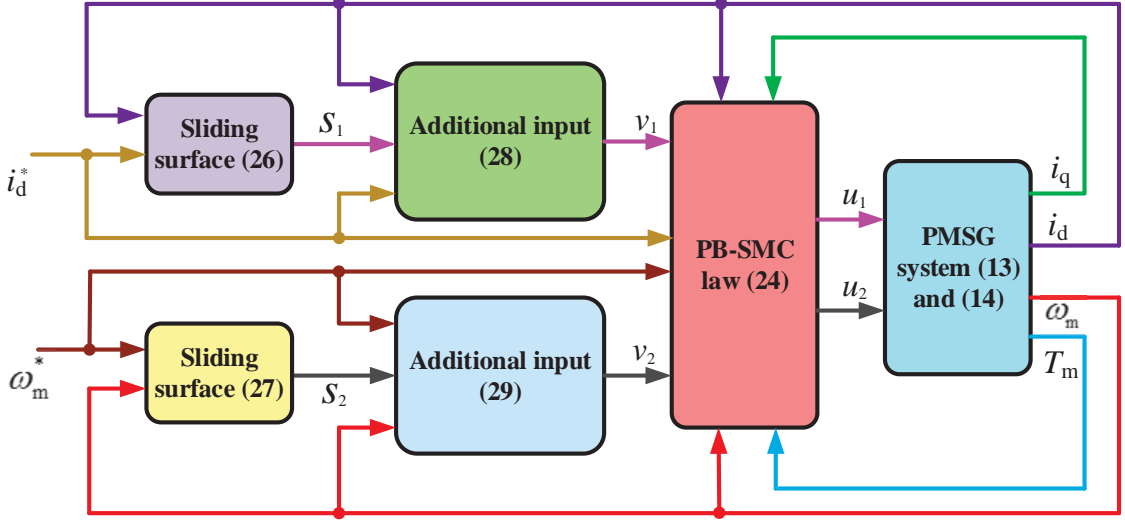


Figure 3: The overall PB-SMC structure of PMSG for MPPT.

are modulated by the sinusoidal pulse width modulation (SPWM) technique [34].

4 Case Studies

The simulation is executed on Matlab/Simulink 7.10 using a personal computer with an IntelR CoreTMi7 CPU at 2.2 GHz and 4 GB of RAM, the PMSG system parameters are taken from reference [33] which are tabulated in Table 1. The proposed PB-SMC is applied on a PMSG based variable speed wind turbine for MPPT, which control performance is compared to that of VC [11], FLC [16], and SMC [20], under four cases, i.e., step change of wind speed, stochastic wind speed variation, pitch angle variation, and robustness against generator parameter uncertainties. Moreover, the PB-SMC parameters are tabulated in Table 2. Consider control inputs may exceed the admissible capacity of generator-side VSC at some operation point, hence their values must be limited, i.e., $|u_1| \leq 0.6$ p.u. and $|u_2| \leq 0.8$ p.u., respectively.

Remark 2. Note that a larger value of control gains ζ_1 , ζ_2 , φ_1 , and φ_2 and sliding surface gains ρ_1 and ρ_2 will result in a faster convergence of sliding surface but with larger control costs; Moreover, a larger value of passivation gains α_1 and α_2 and will inject higher system damping but with larger control costs; Lastly, a larger value of thickness layer boundary ε_1 and ε_2 will lead to a less chattering but with degraded control performance near the sliding surface. The control parameters used in Table 2 are determined by trial-and-error such that a proper trade-off of the above contradictory effects could be achieved.

Table 1: The PMSG system parameters

PMSG rated power	P_{base}	2 MW
radius of wind turbine	R	39 m
air density	ρ	1.205 kg/m ³
rated wind speed	v_{wind}	12 m/s
total inertia	J_{tot}	10000 kg · m ²
field flux	K_e	136.25 V · s/rad
pole pairs	p	11
d-axis stator inductance	L_d	5.5 mH
q-axis stator inductance	L_q	3.75 mH
stator resistance	R_s	50 $\mu\Omega$

Table 2: PB-SMC parameters used in the case studies

control parameters of d-axis current			
$\alpha_1 = 25$	$\zeta_1 = 15$	$\varphi_1 = 10$	$\varepsilon_1 = 0.1$
control parameters of mechanical rotation speed			
$\alpha_2 = 30$	$\zeta_2 = 25$	$\varphi_2 = 15$	$\varepsilon_2 = 0.1$
$\rho_1 = 100$	$\rho_2 = 1$		

4.1 Step change of wind speed

A series of four consecutive step changes of wind speed are applied to briefly mimic a gust, i.e., 8-9 m/s, 9-10 m/s, 10-11 m/s, 11-12 m/s at $t=5$ s, 10 s, 15 s, 20 s, respectively. The MPPT performance of different controllers is provided in Fig. 4. As the wind speed increases sharply, the mechanical power injected into the PMSG grows rapidly thus a power imbalance is resulted in, which then drives an increase of electrical power by accelerating the mechanical rotation speed of wind turbine. Moreover, Fig. 4 clearly illustrates that PB-SMC can extract the optimal wind power as it can maintain the power coefficient closest to its optimum, together with a smooth and rapid mechanical rotation speed compared to that of VC, FLC, and SMC. Additionally, it is worth noting that VC performance degrades considerably at different operation points due to its one-point linearization while the other nonlinear approaches can achieve a globally consistent control performance. Besides, three step changes of d-axis current are also applied to investigate the current regulation performance. It can be clearly observed that VC has a current overshoot during each step change. while PB-SMC can track the current reference at the fastest rate without any overshoot among all controllers.

4.2 Stochastic wind speed variation

A stochastic wind speed variation is simulated to investigate the control performance of the proposed method, in which the wind speed rapidly varies among 7 m/s to 11 m/s in 25 s to mimic a more realistic wind speed in reality [35–37]. The system responses are presented in Fig. 5, from which one can find that

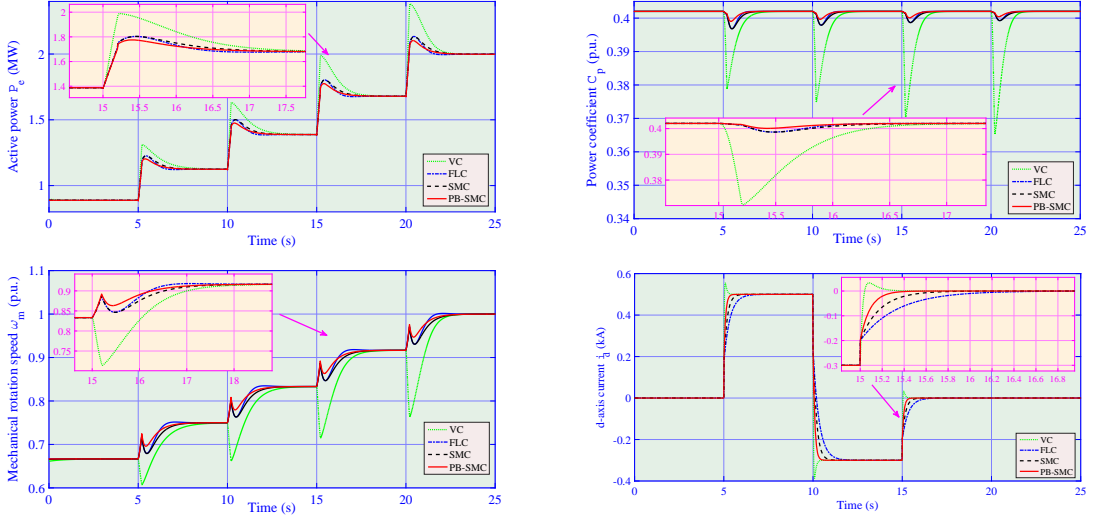


Figure 4: MPPT performance obtained under four consecutive step changes of wind speed from 8 m/s to 12 m/s.

PB-SMC could effectively extract the optimal wind power with the least deviation of power coefficient from its optimum. Again, VC provides the poorest power tracking and it can not achieve a satisfactory performance in the presence of such high-frequency wind speed variation. Besides, SMC outperforms FLC as it owns higher robustness to wind speed uncertainties.

4.3 Pitch angle variation

A pitch angle decrease starts from 2 deg. to 0 deg. in 0.4 s with a constant wind speed of 12 m/s is applied to compare the control performance of PB-SMC to that of others, the performance is given in Fig. 6. It is obvious that PB-SMC can reach the new steady state at the fastest rate thanks to its extra system damping which significantly improves the transient responses. In contrast, the mechanical rotation speed of VC varies dramatically as such operation point shifts from the normal operation condition.

4.4 Robustness against parameter uncertainties

In order to evaluate the robustness against generator parameter uncertainties [38, 39], a series of plant-model mismatches of stator resistance R_s and d-axis inductance L_d with $\pm 20\%$ variation around their nominal value are undertaken, in which a 2 m/s wind speed step increase from 10 m/s is applied. Note that such generator parameter uncertainties might be caused by the temperature variation, wear-and-tear of the generator, measurement errors of apparatus, etc. The peak value of active power $|P_e|$ is recorded for a clear comparison. Fig. 7 illustrates that the variation of $|P_e|$ obtained by VC, FLC, SMC, and

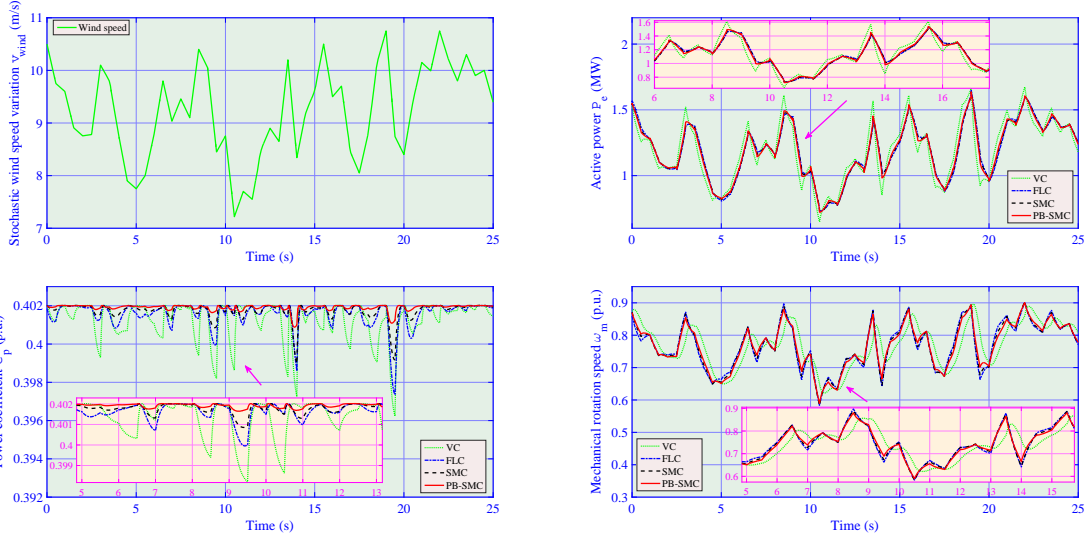


Figure 5: MPPT performance obtained under stochastic wind speed variation among 7 m/s to 11 m/s.

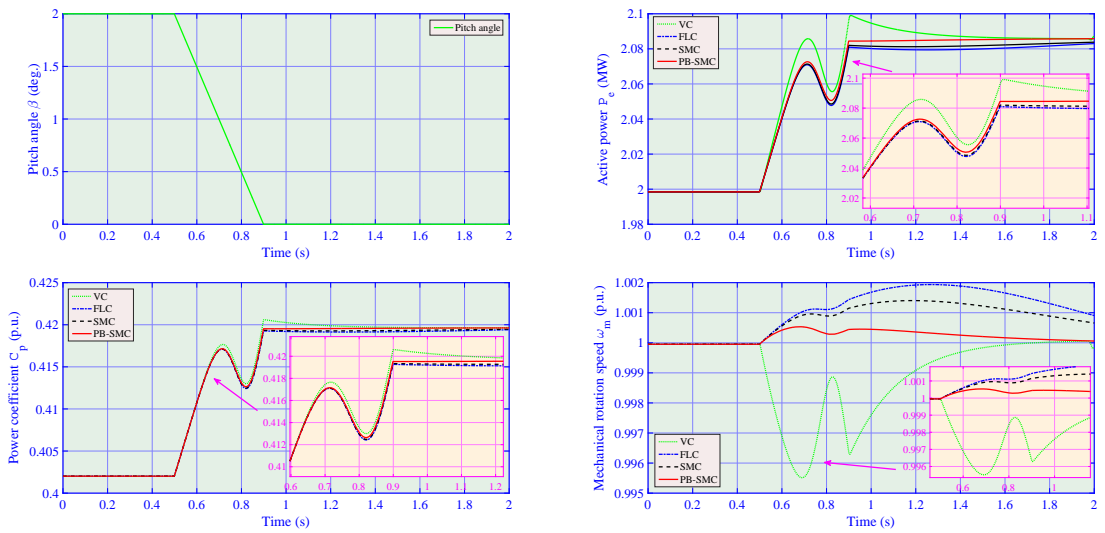


Figure 6: System responses obtained under pitch angle variation reduced from 2 deg. to 0 deg..

PB-SMC is around 17.4%, 28.1%, 9.6%, and 8.1%, respectively. As FLC requires an accurate system model thus it is quite invulnerable to any generator parameter uncertainties. In addition, both SMC and PB-SMC are robust to the generator parameter uncertainties due to the sliding-mode mechanism while PB-SMC performs better than that of SMC thanks to the remained beneficial terms which enhance the system damping.

Table 3: IAE indices (in p.u.) of four controllers obtained in different cases

Control \ Case	Step change of wind speed		Stochastic wind speed variation		Pitch angle variation	
	IAE _{<i>i</i>_d}	IAE _{<i>ω</i>_m}	IAE _{<i>i</i>_d}	IAE _{<i>ω</i>_m}	IAE _{<i>i</i>_d}	IAE _{<i>ω</i>_m}
VC	1.58E-02	3.67E-03	6.17E-03	4.83E-03	3.26E-04	2.18E-04
FLC	1.39E-02	3.24E-03	4.83E-03	2.66E-03	2.86E-04	1.74E-04
SMC	1.31E-02	3.11E-03	3.64E-03	1.97E-03	2.35E-04	1.52E-04
PB-SMC	1.06E-02	2.75E-03	3.12E-03	1.42E-03	2.08E-04	1.26E-04

4.5 Comparative analysis

The integral of absolute error (IAE) indices of each approach calculated in different cases are provided in Table 3, where $IAE_x = \int_0^T |x - x^*| dt$ and x^* is the reference of variable x . The simulation time $T=25$ s. It gives that PB-SMC owns the lowest IAE indices (in bold) in all cases among all controllers. Particularly, its IAE_{*i*_d} obtained in stochastic wind speed variation is just 50.57%, 64.60%, and 85.71% to that of VC, FLC, and SMC, respectively; Besides, its IAE_{*ω*_m} obtained in step change of wind speed is only 67.09%, 76.26%, and 80.92% to that of VC, FLC, and SMC, respectively.

In addition, the real-time variation of storage function $H(i_d, \omega_m, T_e, T_m)$, which describes the system transient responses while a steeper curve indicates a faster error tracking, is demonstrated by Fig. 8. One can observe that PB-SMC has the fastest decrease of storage function and the lowest peak value when a disturbance (wind speed variation or pitch angle variation) occurs. Moreover, the overall integral of storage function $\int_0^T H(i_d, \omega_m, T_e, T_m) dt$ of different cases, which describes the accumulated energy produced by the tracking error while a smaller value means a lower overall tracking error, is compared in Fig. 9. It can be seen that VC has the highest value which means it has the largest accumulated tracking error among all approaches. In contrast, PB-SMC has the minimal accumulated tracking error in all cases.

Lastly, the overall control costs of four controllers required in different cases are presented in Fig. 10. Here, PB-SMC merely requires the lowest control costs in stochastic wind speed variation and pitch angle variation thanks to the careful exploitation of beneficial terms by examining their physical property.

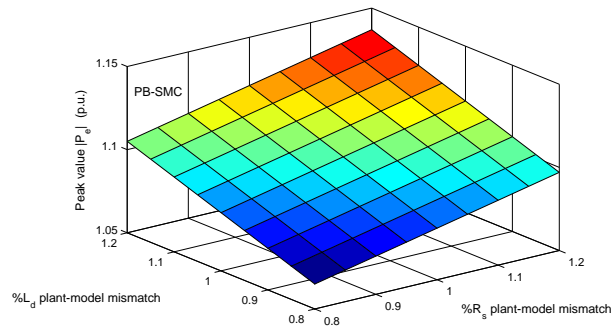
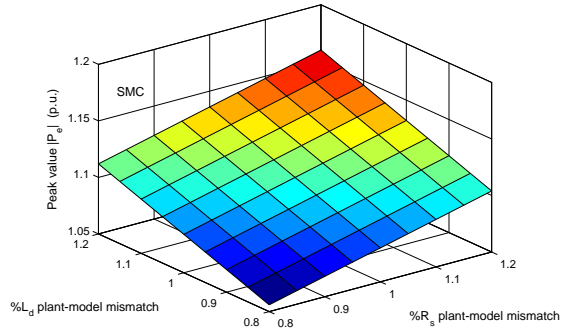
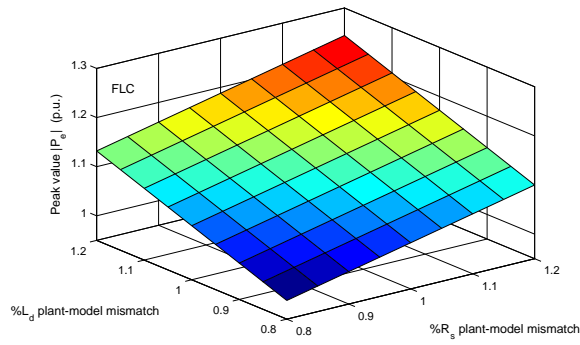
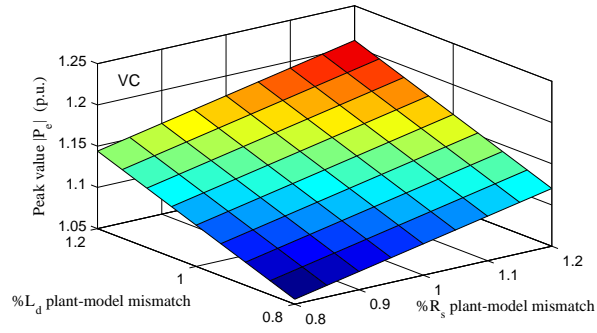


Figure 7: Peak value of active power $|P_e|$ obtained under a 2 m/s wind speed step increase from 10 m/s with 20% variation of the stator resistance R_s and d-axis inductance L_d of different approaches, respectively.

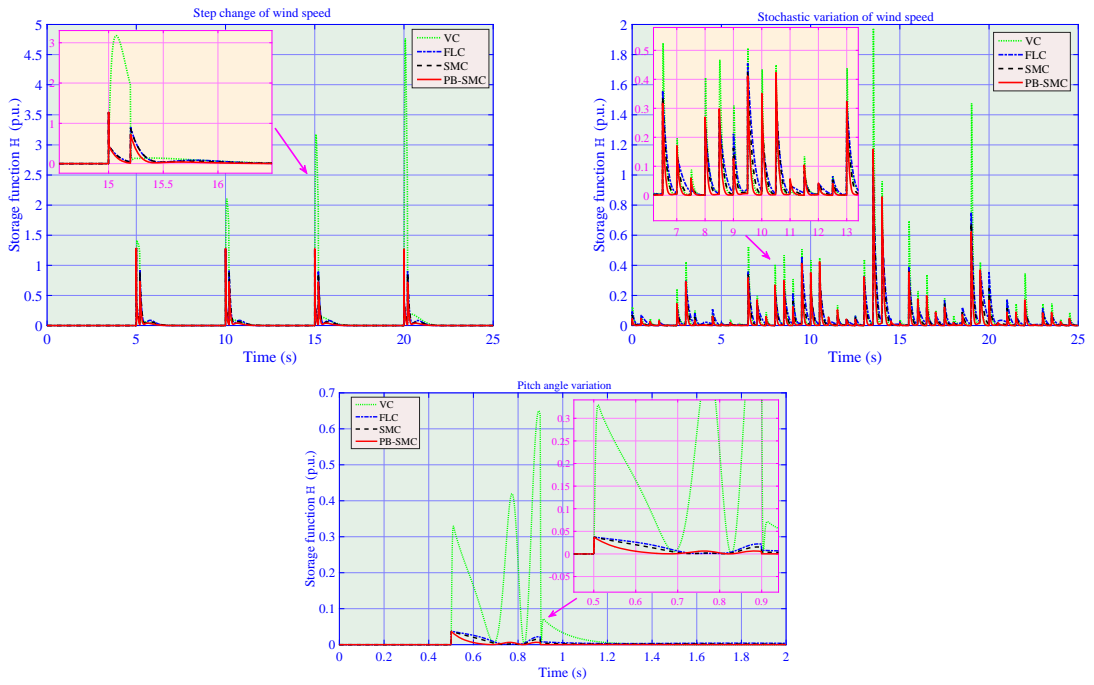


Figure 8: Real-time variation of storage function of four controllers obtained in different cases.

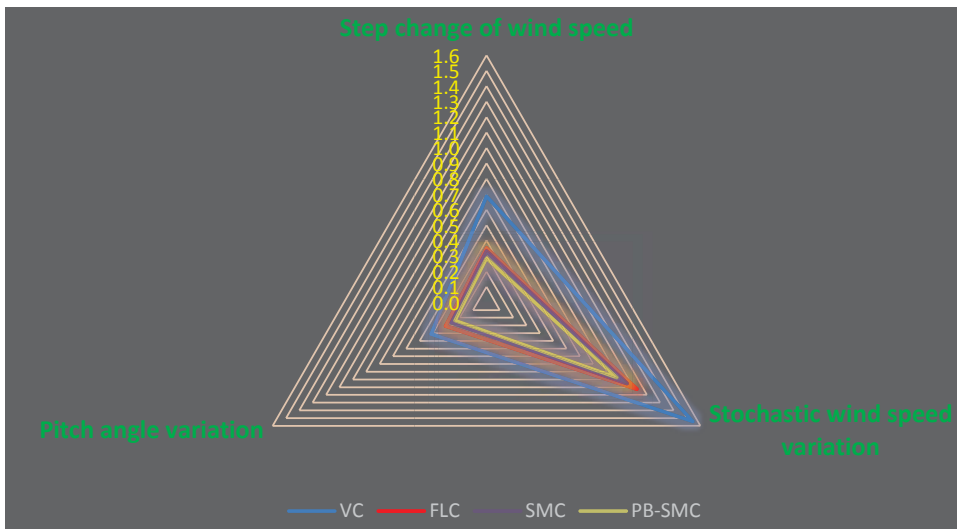


Figure 9: Radar diagram of accumulated storage function of four controllers obtained in different cases.

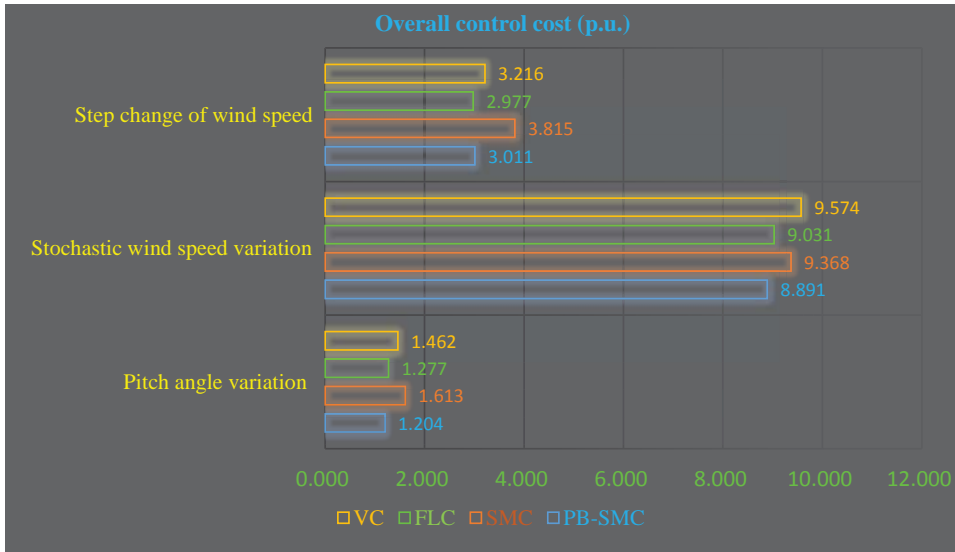


Figure 10: Comparison of overall control costs (in p.u.) of four controllers required in different cases.

Meanwhile, its control costs are just slightly higher than that of FLC and ranks the second lowest among all methods in the step change of wind speed. As a consequence, it can be concluded that PB-SMC is adequate to achieve a satisfactory control performance with reasonable control costs.

5 Hardware-in-the-loop Test

HIL test is an important and powerful technique used in the development and test of complex real-time embedded systems, which provides an effective platform by adding the complexity of the plant under control to the test platform. The complexity of the plant under control is included in test and development by adding a mathematical representation of all related dynamic systems. HIL test has been successfully used in wind energy systems [40–42] to validate the hardware implementation feasibility.

A dSPACE based HIL test is undertaken which configuration and experiment platform are demonstrated by Fig. 11 and Fig. 12, respectively. Here, the PB-SMC based d-axis current controller and mechanical rotation speed controller (28) are implemented on one dSPACE platform (DS1104 board) with a sampling frequency $f_c = 1$ kHz, and the PMSG system is simulated on another dSPACE platform (DS1006 board) with the limit sampling frequency $f_s = 50$ kHz to make HIL simulator as close to the real generator as possible [29, 43]. The measurements of the d-axis current i_d , q-axis current i_q , mechanical rotation speed ω_m , and mechanical torque T_m are obtained from the real-time simulation of the PMSG system on the DS1006 board, which are sent to two controllers implemented on the DS1104 board for the control inputs calculation.

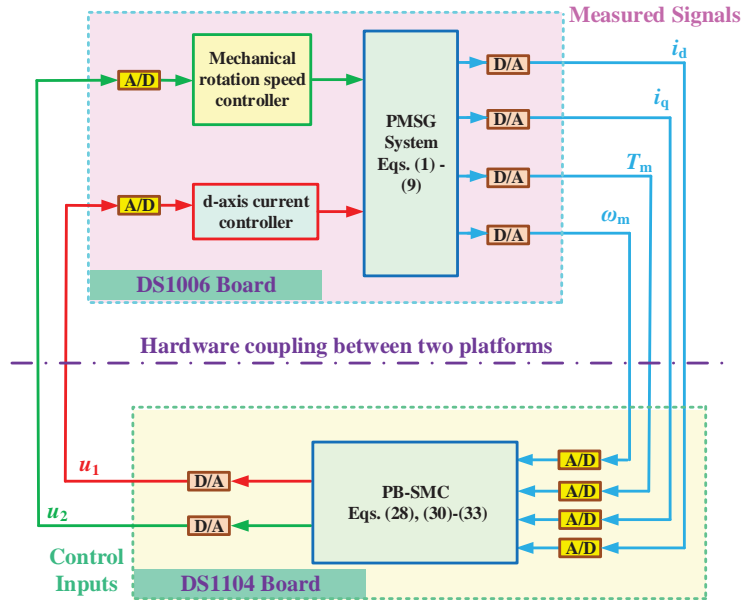


Figure 11: The configuration of the HIL test.

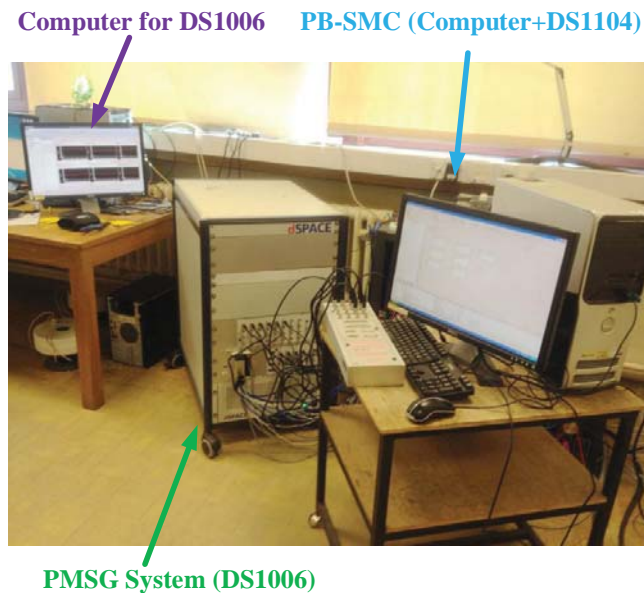


Figure 12: The experiment platform of the HIL test.

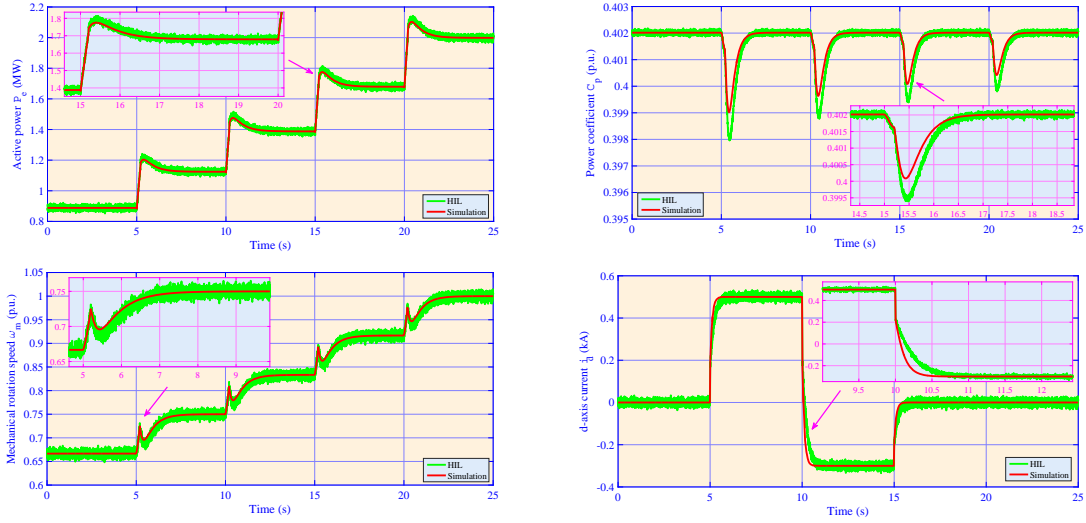


Figure 13: Simulation and HIL test results obtained under four consecutive step changes of wind speed from 8 m/s to 12 m/s.

The HIL tests are performed mainly for two purposes: 1) Validate the correctness and effectiveness of the PB-SMC in real applications; 2) Evaluate the accuracy and real-time computing ability of the PB-SMC based PMSG system in practice.

5.1 HIL Test: Step change of wind speed

The system responses obtained under the simulation and HIL test are compared by Fig. 13 under the same step change of wind speed used in Case Studies. It can be clearly seen that the HIL test has almost the same results as that of the simulation.

5.2 HIL Test: Stochastic wind speed variation

In the presence of the same stochastic wind speed variation of Case Studies, Fig. 14 demonstrates that an optimal power can be effectively extracted while the system responses obtained by the HIL test is similar to that of simulation.

5.3 HIL Test: Pitch angle variation

The same pitch angle variation of Case Studies is applied. One can readily observe from Fig. 15 that the results of the HIL test and simulation match very well.

To this end, the difference of the obtained results between the HIL test and simulation is mainly due to the following three reasons:

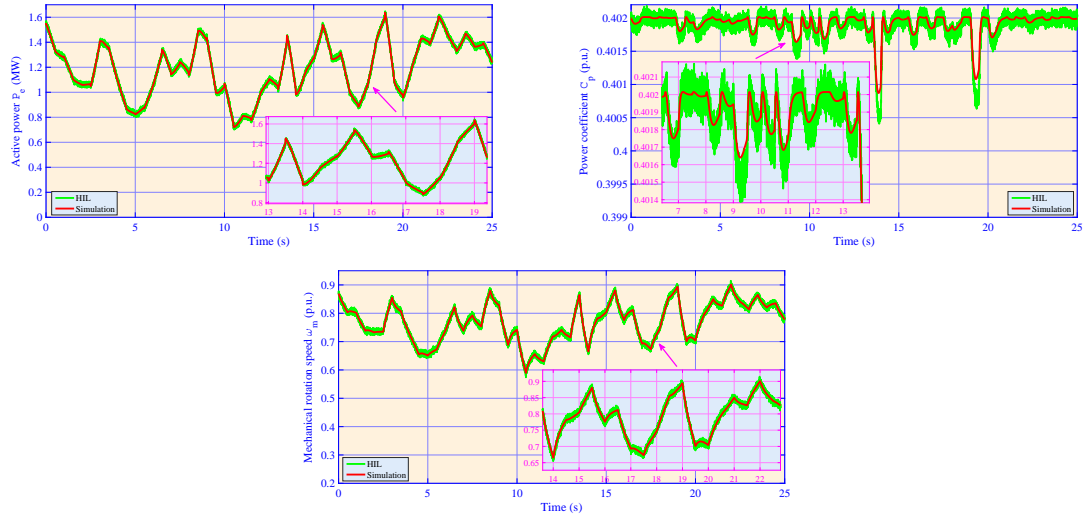


Figure 14: Simulation and HIL test results obtained under stochastic wind speed variation among 7 m/s to 11 m/s.

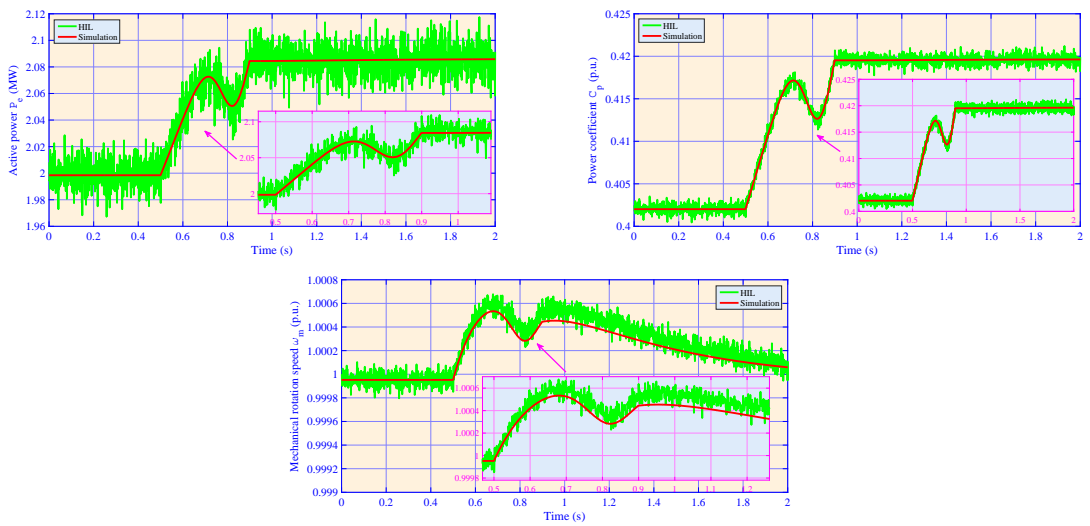


Figure 15: Simulation and HIL test results obtained under pitch angle variation reduced from 2 deg. to 0 deg..

- There exist measurement disturbances in the HIL test which are however not taken into account in the simulation, a filter could be used to remove the measurement disturbances thus the control performance can be improved;
- The discretization of the HIL test and sampling holding may introduce an additional amount of error compared to continuous control used in the simulation;
- The existence of time delay of the real-time controller, which exact value is unlikely to obtain in practice. A time delay $\tau = 2$ ms is assumed in the simulation.

6 Conclusions

A novel PB-SMC is designed in the paper in order to achieve MPPT of a PMSG based variable speed wind turbine. The conclusions can be summarized as the following four aspects:

- (1) Based on the passivity theory, a storage function is constructed in the form of the sum of the resistor heat produced by d-axis current flowing through a virtual unit resistance, kinetic energy of the shaft system, and the accelerating torque energy. Then, its derivative is calculated upon which the role of each term is carefully investigated while the beneficial ones are thus remained to improve the system damping;
- (2) An addition input is introduced to lead the system to be output strictly passive via energy reshaping and to enhance system robustness by employing a SMC, such that PB-SMC is capable of handling various uncertainties;
- (3) Case studies have been undertaken which verify that PB-SMC can rapidly achieve MPPT with the least overshoot under step change of wind speed and stochastic wind speed variation, effectively restore the PMSG system under pitch angle variation, provide significant robustness against generator parameter uncertainties, as well as require relatively low control costs among all cases.
- (4) A dSpace based HIL test has been carried out which validate the implementation feasibility of PB-SMC.

Future studies will be focused on two aspects:

- (a) Apply PB-SMC on both the generator-side converter and grid-side converter to accomplish a complete control design system of PMSG;
- (b) Employ some optimization algorithms to determine the optimal control parameters of PB-SMC.

Acknowledgements

The authors gratefully acknowledge the support of National Natural Science Foundation of China (51477055,51667010,51777078), Yunnan Provincial Talents Training Program (KKSJY201604044), and Scientific Research Foundation of Yunnan Provincial Department of Education (KKJB201704007).

References

- [1] Sagbansua L. and Balo F. ‘Decision making model development in increasing wind farm energy efficiency’, *Renewable Energy*, 109, 354-362, 2017.
- [2] Kaldellis J. K. and Apostolou D. ‘Life cycle energy and carbon footprint of offshore wind energy. Comparison with onshore counterpart’, *Renewable Energy*, 108, 72-84, 2017.
- [3] Liao S. W., Yao W., Han X. N., Wen J. Y., and Cheng S. J. ‘Chronological operation simulation framework for regional power system under high penetration of renewable energy using meteorological data’, *Applied Energy*, 203, 816-828, 2017.
- [4] Liu J., Wen J. Y., Yao W., and Long Y. ‘Solution to short-term frequency response of wind farms by using energy storage systems’, *IET Renewable Power Generation*, 10(5), 669-678, 2016.
- [5] Shen Y., Yao W., Wen J. Y., and He H. B. ‘Adaptive wide-area power oscillation damper design for photovoltaic plant considering delay compensation’, *IET Generation, Transmission & Distribution*, DOI: 10.1049/iet-gtd.2016.2057.
- [6] Yang B., Zhang X. S., Yu T., Shu H. C., and Fang Z. H. ‘Grouped grey wolf optimizer for maximum power point tracking of doubly-fed induction generator based wind turbine’, *Energy Conversion and Management*, 133, 427-443, 2017.
- [7] Xie D., Lu Y. P., Sun J. B., and Gu C. H. ‘Small signal stability analysis for different types of PMSGs connected to the grid’, *Renewable Energy*, 106, 149-164, 2017.
- [8] Tripathi S. M., Tiwari A. N., Singh D. ‘Grid-integrated permanent magnet synchronous generator based wind energy conversion systems: A technology review’, *Renewable and Sustainable Energy Reviews*, 51, 1288-1305, 2015.

- [9] Yang B., Jiang L., Wang L., Yao W., and Wu Q. H. ‘Nonlinear maximum power point tracking control and modal analysis of DFIG based wind turbine’, *International Journal of Electrical Power and Energy Systems*, 74, 429-436, 2016.
- [10] Fernando J. L., Godpromesse K., Francoise L. L. ‘A novel online training neural network-based algorithm for wind speed estimation and adaptive control of PMSG wind turbine system for maximum power extraction’, *Renewable Energy*, 86, 38-48, 2016.
- [11] Li S. H., Haskew T. A., and Xu L. ‘Conventional and novel control designs for direct driven PMSG wind turbines’, *Electric Power Systems Research*, 80(3), 328-338, 2010.
- [12] Alizadeh M. and Shokri K. S. ‘Augmenting effectiveness of control loops of a pmsg (permanent magnet synchronous generator) based wind energy conversion system by a virtually adaptive pi (proportional integral) controller’, *Energy*, 91, 610-629, 2015.
- [13] Hong C. M., Chen C. H., Tu C. S. ‘Maximum power point tracking-based control algorithm for PMSG wind generation system without mechanical sensors’, *Energy Conversion and Management*, 69, 58-67, 2013.
- [14] Antar B., Hacene B., Badreddine B., and Hamza A. ‘Experimental enhancement of fuzzy fractional order PI+I controller of grid connected variable speed wind energy conversion system’, *Energy Conversion and Management*, 123, 569-580, 2016.
- [15] Naggar H. S., Ahmed A. E., and Mohamed E. M. ‘Improved bacterial foraging optimization for grid connected wind energy conversion system based PMSG with matrix converter’, *Ain Shams Engineering Journal*, <http://dx.doi.org/10.1016/j.asej.2017.03.010>.
- [16] Chen J., Jiang L., Yao W., and Wu Q. H. ‘A feedback linearization control strategy for maximum power point tracking of a PMSG based wind turbine’, *International Conference on Renewable Energy Research and Applications*, Madrid, Spain, 20-23 October 2013.
- [17] Youcef S., Sami K., and Mohcene B. ‘Feedback linearization control based particle swarm optimization for maximum power point tracking of wind turbine equipped by PMSG connected to the grid’, *International Journal of Hydrogen Energy*, 41, 20950-20955, 2016.
- [18] Ikram M. H., Mohamed W. N., Najiba M. B. ‘Predictive control strategies for wind turbine system based on permanent magnet synchronous generator’, *ISA Transactions*, 62, 73-80, 2016.

- [19] Yin X. X., Lin Y. G., Li W., Gu Y. J., Liu H. W., and Lei P. F. ‘A novel fuzzy integral sliding mode current control strategy for maximizing wind power extraction and eliminating voltage harmonics’, *Energy*, 85, 677-686, 2015.
- [20] Fernando V. and Roberto D. F. ‘Multiple-input-multiple-output high-order sliding mode control for a permanent magnet synchronous generator wind-based system with grid support capabilities’, *IET Renewable Power Generation*, 9(8), 925-934, 2015.
- [21] Seyed M. M., Maarouf S., Hani V., Handy F. B., and Mohsen S., ‘Sliding mode control of PMSG wind turbine based on enhanced exponential reaching law’, *IEEE Transactions on Industrial Electronics*, 63(10), 6148-6159, 2016.
- [22] Riad A., Toufik R., Djamila R., and Abdelmounaim T. ‘Robust nonlinear predictive control of permanent magnet synchronous generator turbine using Dspace hardware’, *International Journal of Hydrogen Energy*, 41, 21047-21056, 2016.
- [23] Fantino R., Solsona J., and Busada C. ‘Nonlinear observer-based control for PMSG wind turbine’, *Energy*, 113, 248-257, 2016.
- [24] Wei C., Zhang Z., Qiao W., and Qu L. Y. ‘An adaptive network-based reinforcement learning method for MPPT control of PMSG wind energy conversion systems’, *IEEE Transactions on Power Electronics*, 31(11), 7837-7848, 2016.
- [25] Ortega R., Schaft A., Mareels I., and Maschke B., ‘Putting energy back in control’, *IEEE Control Systems*, 21(2), 18-33, 2001.
- [26] Pena R. R., Fernandez R. D., Mantz R. J. ‘Passivity control via power shaping of a wind turbine in a dispersed network’, *International Journal of Hydrogen Energy*, 39, 8846-8851, 2014.
- [27] Santos G. V., Cupertino A. F., Mendes V. F., and Seleme S. I. ‘Interconnection and damping assignment passivity-based control of a PMSG based wind turbine for maximum power tracking’, *2015 IEEE 24th International Symposium on Industrial Electronics (ISIE)*, Buzios, 306-311, 2015.
- [28] Yang B., Jiang L., Yao W., and Wu Q. H. ‘Perturbation observer based adaptive passive control for damping improvement of VSC-MTDC systems’, *Transactions of the Institute of Measurement and Control*, 39(9), 1409-1420, 2017.
- [29] Yang B., Jiang L., Yao W., and Wu Q. H. ‘Perturbation estimation based coordinated adaptive passive control for multimachine power systems’, *Control Engineering Practice*, 44, 172-192, 2015.

- [30] Donairea A., Romeroc J. G., Perezd T. ‘Trajectory tracking passivity-based control for marine vehicles subject to disturbances’, *Journal of the Franklin Institute*, 354, 2167-2182, 2017.
- [31] Mojallizadeh M. R., Badamchizadeh M. A. ‘Power management of PV/battery hybrid power source via passivity-based control’, *Renewable Energy*, 36, 2440-2450, 2011.
- [32] Ayad M. Y., Becherif M., Henni A., Aboubou A., Wack M., and Laghrouche S. ‘Passivity-based control applied to DC hybrid power source using fuel cell and supercapacitors’, *Energy Conversion and Management*, 51(7), 1468-1475, 2010.
- [33] Uehara A., Pratap A., Goya T., Senjyu T., Yona A., Urasaki N., and Funabashi T. ‘A coordinated control method to smooth wind power fluctuations of a PMSG-based WECS’, *IEEE Transactions on Renewable Energy*, 26(2), 550-558, 2011.
- [34] Faraji F., Mousavi S. M., Hajirayat A., Birjandi A. A. M., AlHaddad K. ‘Single-stage single-phase three-level neutral-point-clamped transformerless grid-connected photovoltaic inverters: Topology review’, *Renewable Energy* 80, 197-214, 2017.
- [35] Yang B., Yu T., Shu H. C., Dong J., Jiang L. ‘Robust sliding-mode control of wind energy conversion systems for optimal power extraction via nonlinear perturbation observers’, *Applied Energy*, <http://dx.doi.org/10.1016/j.apenergy.2017.08.027>
- [36] Yang B., Hu Y. L., Huang H. Y., Shu H. C., Yu T., Jiang L. ‘Perturbation estimation based robust state feedback control for grid connected DFIG wind energy conversion system’, *International Journal of Hydrogen Energy*, vol. 42, no. 33, pp. 20994-21005, 2017.
- [37] Yang B., Yu T., Zhang X. S., Huang L. N., Shu H. C., Jiang L. ‘Interactive teaching-learning optimizer for parameter tuning of VSC-HVDC systems with offshore wind farm integration’, *IET Generation, Transmission & Distribution*. DOI: 10.1049/iet-gtd.2016.1768
- [38] Yao W., Jiang L., Wen J. Y., Wu Q. H., and Cheng S. J. ‘Wide-area damping controller for power system inter-area oscillations: a networked predictive control approach’, *IEEE Transactions on Control Systems Technology*, 23(1), 27-36, 2015.
- [39] Shen Y., Yao W., Wen J. Y., He H. B., and Chen W. B. ‘Adaptive supplementary damping control of VSC-HVDC for interarea oscillation using GrHDP’, *IEEE Transactions on Power Systems*, DOI: 10.1109/TPWRS.2017.2720262.

- [40] Li H., Steurer M., Shi K. L., Woodruff S., Zhang D. ‘Development of a unified design, test, and research platform for wind energy systems based on hardware-in-the-loop real-time simulation’, *IEEE Transactions on Industrial Electronics*, vol. 53, no. 4, pp. 1144-1151, 2006.
- [41] Hasanzadeh A., Edrington C. S., Stroupe N., and Bevis T. ‘Real-time emulation of a high-speed microturbine permanent-magnet synchronous generator using multiplatform hardware-in-the-Loop realization’, *IEEE Transactions on Industrial Electronics*, vol. 61. no. 6, pp. 3109-3118, 2014.
- [42] Huerta F., Tello R. L., and Prodanovic M. ‘Real-time power-hardware-in-the-loop implementation of variable-speed wind turbines. ’, *IEEE Transactions on Industrial Electronics*, vol. 64, no. 3, pp. 1893-1904, 2017.
- [43] Yang B., Sang Y. Y., Shi K., Yao W., Jiang L., and Yu T. ‘Design and real-time implementation of perturbation observer based sliding-mode control for VSC-HVDC systems’, *Control Engineering Practice*, vol. 56, pp. 13-26, 2016.